Supporting Information

Targeted metabolic glycoengineering using multivalent mannosyl metal-organic frameworks (MOFs)

Pei-Hong Tong,[a‡] Chen Guo,[ac‡] Xi-Le Hu,[a] Tony D. James,[de*] Jia Li [c*] and Xiao-Peng He [ab*]

[a] *Key Laboratory for Advanced Materials and Joint International Research Laboratory of Precision Chemistry and Molecular Engineering, Feringa Nobel Prize Scientist Joint Research Center, Frontiers Center for Materiobiology and Dynamic Chemistry, School of Chemistry and Molecular Engineering, East China University of Science and Technology, 130 Meilong Rd., Shanghai 200237, China.*

[b] *The International Cooperation Laboratory on Signal Transduction, National Center for Liver Cancer, Eastern Hepatobiliary Surgery Hospital, Shanghai 200438, China.*

[c] *State Key Laboratory of Chemical Biology, Shanghai Institute of Materia Medica, Chinese Academy of Sciences, Shanghai, 201203 China.*

[d] *Department of Chemistry, University of Bath, Claverton Down, Bath BA2 7AY, UK*

[e] *School of Chemistry and Chemical Engineering, Henan Normal University, Xinxiang 453007, China.*

‡These authors contributed equally to this work.

***Corresponding authors.**

t.d.james@bath.ac.uk (T. D. James)

jli@simm.ac.cn (J. Li)

xphe@ecust.edu.cn (X.-P. He)

Contents list

S1. Experimental procedures

S2. Additional figures and tables

S3. Spectra of new compounds

S4. Additional references

S1. Experimental procedures

General. 1,2,3,4,6-Penta-O-acetyl-α-D-mannopyranose and hydroxybenzoic acid were purchased from Shanghai Kaiwei Chemical Technology Co. **ManNAz** (**AMN**) was purchased from Shanghai Aladdin Co. Concanavalin A (Con A), peanut agglutinin (PNA), and bovine serum albumin (BSA) were purchased from Shanghai Aladdin Biochemical Technology Co. Other chemicals and reagents were purchased commercially at analytical grade unless otherwise noted. ^{1}H NMR and ^{13}C NMR spectra were recorded on a Bruker AM 400 MHz spectrometer and an Ascend 600 spectrometer with tetramethylsilane (TMS) as the internal reference, respectively. High-resolution transmission electron microscopic (HRTEM) images were obtained using JEOL 2100. Fluorescence microscopy was performed on an Operetta high content imaging system and quantified by the Columbus image data analysis system (Perkin Elmer, USA). Analytical high performance liquid chromatograph (HPLC) was carried out on a Shimadzu Nexera LC-40 HPLC System equipped with a VWD UV-Vis detector, and a ZORBAX Eclipse XDB-C18 column (Analytical, 4.6 × 150 mm). Dynamic light scattering (DLS) was carried out using a LB-550 DLS Nano-Analyzer (Horiba, Japan). Powder X ray diffraction (XRD) was carried out using a X-ray Diffractometer Smartlab SE (Rigaku, Japan).

Synthesis of the Man-L1 and Man-L2 ligands.

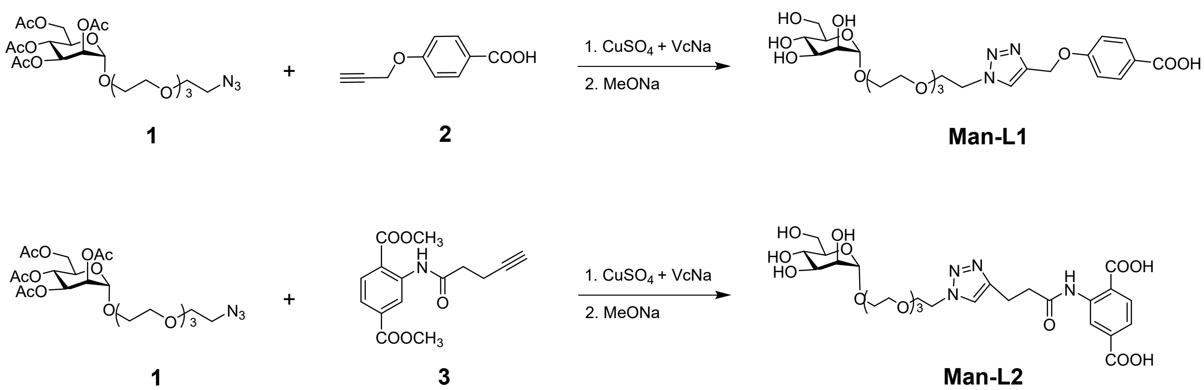

Scheme S1. Synthetic route to **Man-L1** and **Man-L2**.

Synthesis of 3 (Compounds 1[1] and 2[2] were synthesized according to previous literature reports).

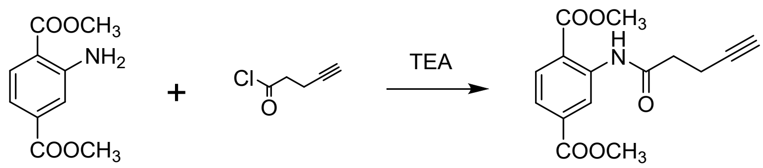

3

Pentynoic acid (1.0 g, 10.0 mmol) and DMF (0.007 g, 0.1 mmol) were added to anhydrous sulfoxide chloride solution (4 mL) and stirred at room temperature for 2 h until depletion of the reactants. Solvent was removed in vacuum to give a faint yellow oil (Intermediate 1). Then, dimethyl aminoterephthalate (500 mg, 2.4 mmol), intermediate 1 (580 mg, 5 mmol), and triethylamine (486 mg, 5 mmol) were added to anhydrous CH_2Cl_2 (20 mL) and stirred overnight at room temperature until the reactants were depleted. The organic phase was washed with distilled water and brine, the organic phase was concentrated in vacuum to give a residue, which was purified on a silica gel column (PE/EA = 4:1) to give the yellow solid (465 mg, 74%). ^{1}H NMR (400 MHz, $CDCl_3$) δ 11.10 (s, 1H), 9.35 (d, J = 1.6 Hz, 1H), 8.10 (d, J = 8.3 Hz, 1H), 7.75 (dd, J = 8.3, 1.7 Hz, 1H), 3.95 (d, J = 11.7 Hz, 6H), 2.73–2.69 (m, 2H), 2.67–2.63 (m, 2H), 2.01 (t, J = 2.6 Hz, 1H). ^{13}C NMR (151 MHz, $CDCl_3$) δ 169.8, 168.1, 166.0, 141.2, 135.4, 130.8, 123.3, 121.3, 118.1, 82.5, 69.3, 52.7, 52.5, 37.0, 14.5. HRMS (ESI, *m/z*): $[M + Na]^+$ calcd for $C_{15}H_{15}NNaO_5$ 312.0848, found 312.0849.

Synthesis of Man-L1 and Man-L2.

To a solution of azide **1** in a mixed solution of tetrahydrofuran (THF) (5 mL) and water (2 mL), alkyne **2** or **3**, aqueous $CuSO_4 \cdot 5H_2O$, and aqueous sodium ascorbate (VcNa) was added, and the mixture was stirred for 12 h at room temperature. THF was removed in vacuum, and then water (20 mL) was added to dilute the concentrate, followed by extraction with ethyl acetate (3 × 20 mL). The combined organic layers were dried with $MgSO_4$, filtered, and then concentrated in vacuum to obtain a residue, which was purified through a silica gel column (PE/EA = 1:4) to give intermediate as white solid. This intermediate was directly dissolved in anhydrous methyl alcohol (5 mL), and then freshly prepared sodium methanol solution (1 mL, 2 mol L^{-1}) was added to the mixture under ice bath. The mixture was stirred for 2 h at room temperature. Then, the pH of the solution was adjusted to neutral by addition of ion exchange resin. After filtration and concentration in vacuum, the resulting residue was purified through column chromatography on C18 phase to give **Man-L1** or **Man-L2** as a yellow oil.

Man-L1. From **1** (100 mg, 0.18 mmol), **2** (48 mg, 0.27 mmol), $CuSO_4{\cdot}5H_2O$ (10 mg, 0.06 mL), VcNa (40 mg, 0.2 mL), column chromatography on C18 phase (H_2O/MeOH = 4:1, v/v) obtained **Man-L1** as a yellow oil (42 mg, 86%). ^{1}H NMR (400 MHz, MeOD) δ 8.22 (s, 1H), 7.99 (d, J = 8.9 Hz, 2H), 7.10 (d, J = 8.9 Hz, 2H), 5.28 (s, 2H), 4.78 (d, J = 1.7 Hz, 1H), 4.64–4.61 (m, 2H), 3.92–3.89 (m, 2H), 3.82–3.77 (m, 3H), 3.71 (d, J = 5.6 Hz, 1H), 3.69–3.67 (m, 1H), 3.63 (d, J = 2.7 Hz, 1H), 3.62–3.59 (m, 6H), 3.59–3.53 (m, 8H); ^{13}C NMR (151 MHz, MeOD) δ 168.1, 162.0, 142.5, 131.4, 125.2, 123.2, 114.1, 100.2, 73.1, 71.1, 70.6, 70.1, 70.0, 70.0, 69.9, 69.8, 68.7, 67.1, 66.2, 61.4, 60.8, 50.2. HRMS (ESI, *m/z*): $[M + H]^+$ calcd for $C_{24}H_{35}N_3O_{12}$ 580.2118, found 580.2119.

Man-L2. From **1** (100 mg, 0.18 mmol), **3** (78 mg, 0.27 mmol), $CuSO_4{\cdot}5H_2O$ (10 mg, 0.06 mL), VcNa (40 mg， 0.202 mL), column chromatography on C18 phase (H_2O/MeOH = 4:1, v/v) obtained **Man-L2** as a yellow oil (35 mg, 85%). ^{1}H NMR (400 MHz, MeOD) δ 9.22 (t, J = 1.9 Hz, 1H), 8.16 (dd, J = 8.3, 1.8 Hz, 1H), 7.91 (s, 1H), 7.77–7.73 (m, 1H), 4.81 (d, J = 1.7 Hz, 1H), 4.56 (t, J = 5.0 Hz, 2H), 3.95 (s, 1H), 3.89–3.80 (m, 6H), 3.75–3.67 (m, 3H), 3.66–3.57 (m, 9H), 3.57–3.50 (m, 7H), 3.15 (t, J = 7.2 Hz, 2H), 2.89 (t, J = 7.2 Hz, 2H); ^{13}C NMR (151 MHz, MeOD) δ 171.2, 169.0, 167.1, 145.7, 140.7, 135.3, 131.1, 131.0, 123.2, 123.1, 122.9, 121.2, 100.2, 73.1, 71.0, 70.6, 70.1, 70.0, 69.9, 69.9, 68.9, 67.1, 66.2, 61.4, 50.0, 36.8, 20.5. HRMS (ESI, *m/z*): $[M + H]^+$ calcd for $C_{27}H_{38}N_4O_{14}$ 643.2463, found 643.2464.

Preparation of MIL-101-Man1 and MIL-101-Man2

To a solution of 2-aminoterephthalic acid (36 mg, 0.20 mmol) and **Man-L1** (or **Man-L2**) (26 mg, 0.04 mmol) in 5 mL DMF, metallic precursor $FeCl_3{\cdot}6H_2O$ (100 mg, 0.4 mmol) was added. The resulting mixture was sonicated for 10 min, and then heated at 60 °C for 24 h. The resulting suspension was centrifuged (8000 rpm, 15 min), and the crude precipitate was washed sequentially with DMF (10 mL), deionized water (10 mL) and acetone (10 mL). This was followed by centrifugation and drying under a vacuum to obtain 36 mg of **MIL-101-Man1** (or 33 mg of **MIL-101-Man2**) as a brown solid.

Preparation of AMN/MIL-101-Man1 and AMN/MIL-101-Man2

MIL-101-Man1 (or **MIL-101-Man2**) (5 mg) was added to a flask containing 1 mL MeOH solution of **AMN** (2 mg mL^{-1}) at room temperature. The mixture was stirred at 500 rpm for 24 h, centrifuged at 8000 rpm for 10 min, and then washed three times with water (10 mL per wash). The resulting precipitate was dried under a vacuum to obtain **AMN/MIL-101-Man1** (or **AMN/MIL-101-Man2**) as a brown solid. The loading amount of **AMN** in **MIL-101-Man1** (or **MIL-101-Man2**) was determined using HPLC. Note: The above steps need to be operated under aseptic conditions. **AMN/MIL-101-Man** was stored at 4 °C prior to use, and the concentration described for **AMN/MIL-101-Man** are based on **AMN**.

Dynamic light scattering (DLS)

After incubation of 0.1 mg mL^{-1} **AMN/MIL-101-Man** with different concentrations of Con A, PNA or BSA (0, 10 and 50 μg mL^{-1}) in 10 mM HEPES (pH 7.4, containing 150 mM NaCl, 1 mM $MnCl_2$, 1 mM $CaCl_2$) for 10 min, the hydrodynamic diameters of the resulting mixtures were analyzed on a Horiba LB-550 DLS nano- analyzed.

Stability of AMN/MIL-101-Man

Changes in hydrodynamic diameter of **AMN/MIL-101-Man** were measured after incubating 0.1 mg mL^{-1} of **AMN/MIL-101-Man** in different solutions (including a pH 5.6 PBS solution, pH 7.4 PBS solution, or a culture medium at 37 °C) for 12 or 24 h by DLS.

Determination of sugar content using the anthrone–sulfuric acid method.

In a beaker kept in the dark, anthrone (0.1 g) was gradually mixed with sulfuric acid (20 mL) with constant stirring using a magnetic stirrer until complete dissolution. Using the anthrone–sulfuric acid method, a standard curve was plotted with different concentrations of free mannose (20, 40, 60, 80 and 100 ng mL^{-1}). Briefly, different concentrations of free mannose or an **AMN/MIL-101-Man** solution (0.5 mL, 0.1 mg mL^{-1}) were added to a glass tube, followed by the addition of anthrone–sulfuric acid (1 mL). The tube was covered with aluminum foil, and heated at 80 °C for 20 min. The resulting mixtures were cooled to room temperature and their UV-vis absorption at 620 nm was determined. The mannose content on the surface of **AMN/MIL-101-Man** was calculated using the standard linear equation plotted for free mannose shown in Figure S2.

Measurement of AMN release by HPLC.

AMN/ MIL-101-Man2 was dissolved in PBS of different pH (7.4 or 5.6) for 24 h. The amount of **AMN** released from **AMN/MIL-101-Man2** with time was measured by HPLC. In brief, the release amount was calculated by the following equation: $M_r/M_t \times 100\%$, where M_t is the total amount of **AMN** loaded in **MIL-101-Man2**, and M_r is the cumulative amount of **AMN** released at different time points.

Cell Culture

Triple negative breast cancer cell line MDA-MB-231 and human cervical cancer cell line HeLa were obtained from ATCC. Both cells were cultured in DMEM-HG medium supplemented with 10% fetal bovine serum (FBS), 0.1% Penicillin-Streptomycin Solution at 37 °C in a humidified atmosphere containing 5% CO_2 and 95% air. Cells were split when reaching 80% confluency.

Cellular uptake of MOFs measured by Inductively coupled plasma-Mass Spectrometry (ICP-MS).

MDA-MB-231 cells were seeded into 6-well plates and incubated for 24 h. Then, cells were incubated with **AMN/MIL-101-Man2** (20 μM/36 μg mL^{-1}) for 2 h or 4 h in 1.5 mL of culture medium. After incubation, **AMN/MIL-101-Man2** was removed, and cells were washed three times with PBS and lysed with trypsin. The resulting cell lysates were resuspended in 0.5 mL PBS. After cell counting with a cell-counting board, the cells were then mixed with 1 mL of concentrated nitric acid and incubated at 65 °C overnight. After dilution in 5 mL of water, the levels of Fe in cells were measured by ICP-MS (Agilent 7900).

Bioorthogonal glycan labelling

Cells were seeded in a black 96-well microplate with optically clear bottom and cultured overnight. MDA-MB-231 and HeLa cells were incubated for 24 h with **AMN**, **AMN/MIL-101**, **AMN/MIL-101-Man1, AMN/MIL-101-Man2** or **MIL-101-Man2**. The cell-surface azides were then fluorescently labeled by 10 μM **DBCO-FITC** in serum-free medium for 30 min at 37 °C. Subsequently, cells were incubated with Hoechst 33342 (5 μg mL^{-1}) for 10 min and rinsed by PBS three times. The fluorescence images were recorded using an Opera Phenix high content imaging system (Perkinelmer, US) and then quantified using a Columbus™ Image Data Storage and Analysis System. The excitation/emission channels used for **DBCO-FITC** and Hoechst 33342 were 488/500-550 nm and 405/435-480 nm, respectively. In the time-dependent imaging experiments, media containing **AMN/MIL-101-Man2** were replaced with fresh medium at different indicated time points, and the cells were cultured for another 24 h prior to imaging.

Co-culture experiment

Lentiviral packaging of pLKO.1-mCherry-Puro and pLKO.1-TagBFP-Puro were performed using Lenti-293T cells. MDA-MB-231 and HeLa cells were infected with pLKO.1-mCherry-Puro-derived lentivirus and pLKO.1-TagBFP-Puro-derived lentivirus for 48 hr, respectively. Then, a puromycin (2 μg mL^{-1}) selection procedure was run for a week to establish the cell lines stably expressing the target fluorescent protein (mCherry-MDA-MB-231 and TagBFP-HeLa). A mixture of the two established cell lines with a proportion of 1:1 was co-cultured in growth medium supplemented with 10% FBS and seeded to a 24-well microplate with coverslip overnight. **AMN/MIL-101-Man2** (20 μM/36 μg mL^{-1}) or **AMN/ MIL-101** (20 μM/35 μg mL^{-1}) were added to the co-culture cells for 24 hr, followed by labeling with **DBCO-FITC**. Cells were rinsed twice with PBS and fixed with 4% paraformaldehyde for 15 min at room temperature. After sealing, the fluorescence was imaged using a confocal laser-scanning microscope (Leica TCS SP8, Leica Microsystems, Wetzlar, Germany) and the images were quantified by the software, Image J. The excitation/emission channels used for mCherry, TagBFP and **DBCO-FITC** were 561/580-620nm, 405/435-480 nm and 488/500-550 nm, respectively.

Cell Viability

Cells were seeded in a 96-well plate with 100 μL medium and cultured for 24 h prior to treatment with **AMN/MIL-101-Man1** or **AMN/MIL-101-Man2** at different concentrations. After 24 h, the cell viability was measured using the CellTiter 96® AQueous Non-Radioactive Cell Proliferation Assay (MTS) (Promega) on a microplate reader. Briefly, the original medium was replaced with a serum-free medium and then 10 μL MTS was added to each well. After incubation for 30 min at 37 °C, the absorbance at 490 nm was measured and normalized to that of control cells without treatment with the MOFs. The optical density of the result was directly proportional to the number of viable cells. The experiments were performed in triplicate.

Immunofluorescence staining

Cells were seeded in a black 96-well microplate with optically clear bottom and cultured overnight. Then, cells were fixed with 4% paraformaldehyde at room temperature for 20 min followed by blocking with 5% BSA at room temperature for 1 hr. Then, cells were continuously incubated with anti-CD206 primary antibody at 4 °C overnight. Afterwards, cells were washed with PBS 3 times and incubated with a fluorescent secondary antibody (1:500 diluted by PBS) at room temperature for 1 h. Finally, the cells were rinsed with PBS 3 times and incubated with Hoechst (5 μg mL^{-1}) for 10 min. After replacing the medium with PBS, the fluorescence images were recorded using an Opera Phenix high content imaging system (Perkinelmer, US) and then quantified using a Columbus™ Image Data Storage and Analysis System.

CD206 siRNA knockdown

Transfection of siRNA reagents was done with Lipofectamine™ 2000 Transfection Reagents (Invitrogen 11668500) at 40 pM per well in a 24-well microplate. After 48 h of transfection, cells were harvested for imaging experiments.

The siRNA sequence for CD206 is as below:

sense: GCUUGUGUUUCAAGCUGUAUG

antisense: UACAGCUUGAAACACAAGCUU

Statistics

In this study, the differences between experimental and control groups were analyzed using one-way ANOVA and considered statistically significant (marked with an asterisk (*) in all figures) if $p < 0.01$.

S2. Additional figures

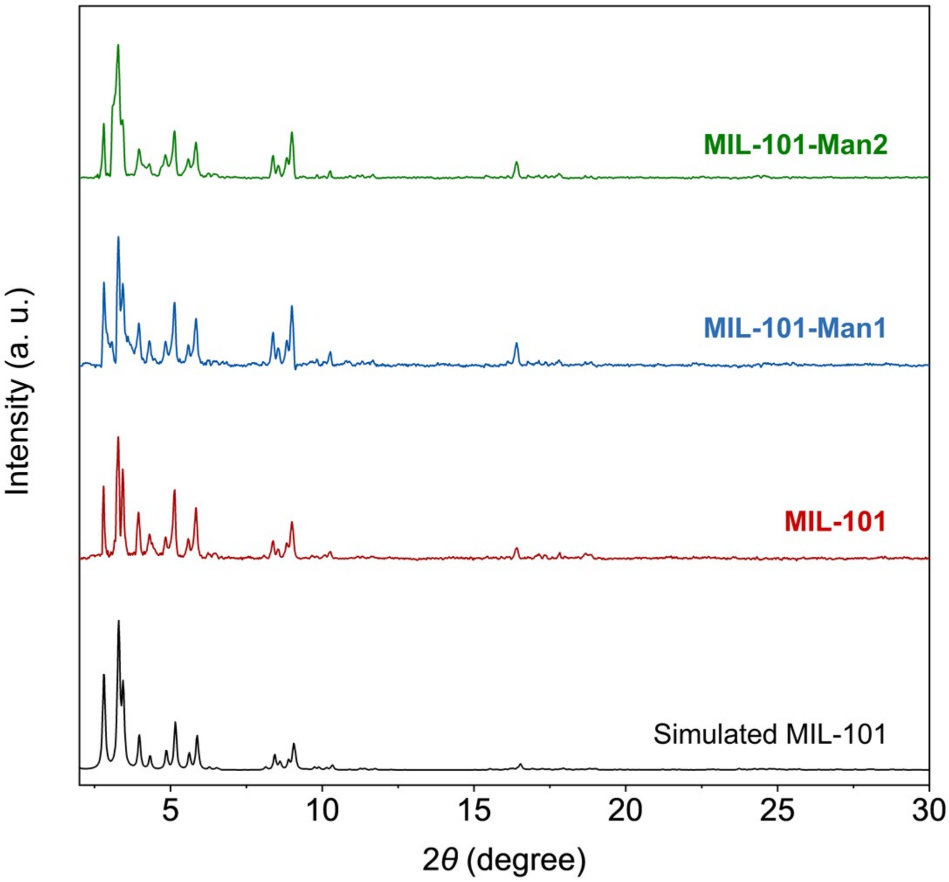

Figure S1. Powder XRD diffraction patterns of simulated MIL-101, and as-prepared **MIL-101** (10 mg), **MIL-101-Man1** (10 mg) and **MIL-101-Man2** (10 mg).

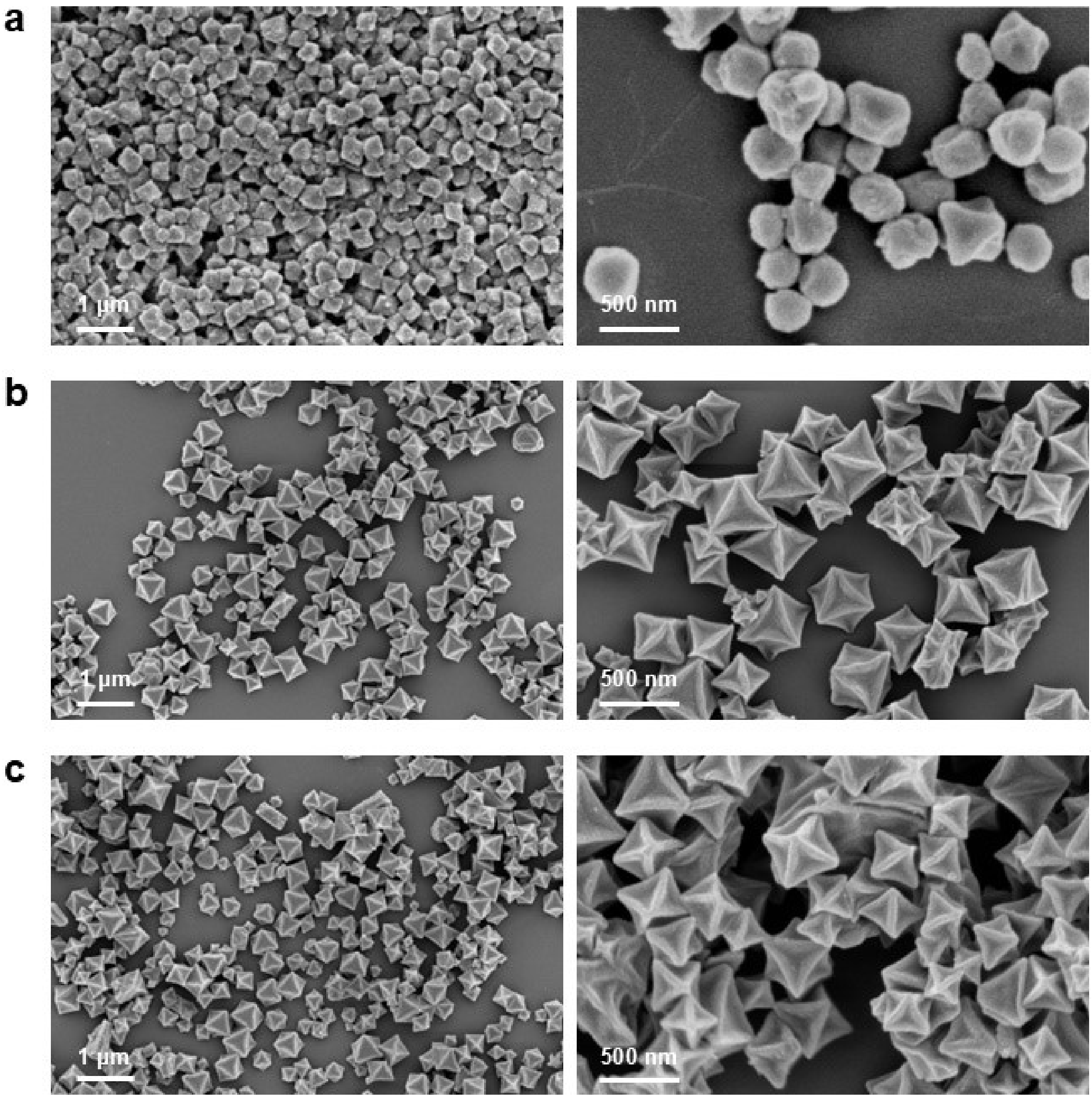

Figure S2. SEM Images of (a) **MIL-101** (0.1 mg mL^{-1}), (b) **MIL-101-Man1** (0.1 mg mL^{-1}) and (c) **MIL-101-Man2** (0.1 mg mL^{-1}).

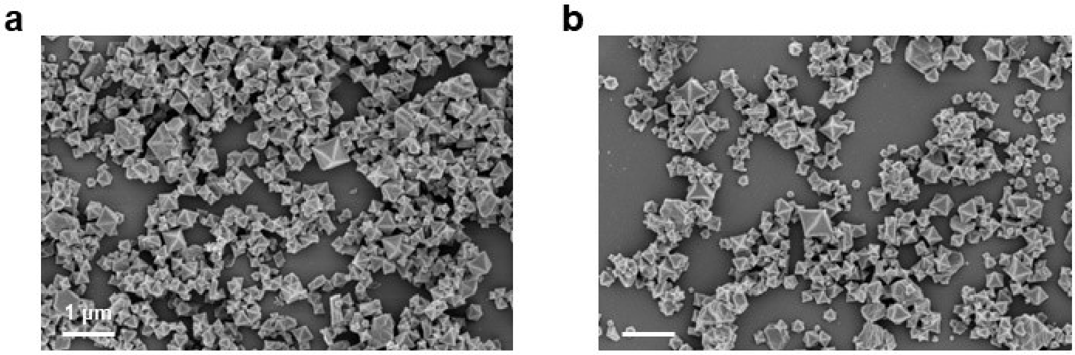

Figure S3. SEM Images of (a) **MIL-101-Man1** (0.1 mg mL^{-1}) and (b) **MIL-101-Man2** (0.1 mg mL^{-1}) from a different batch.

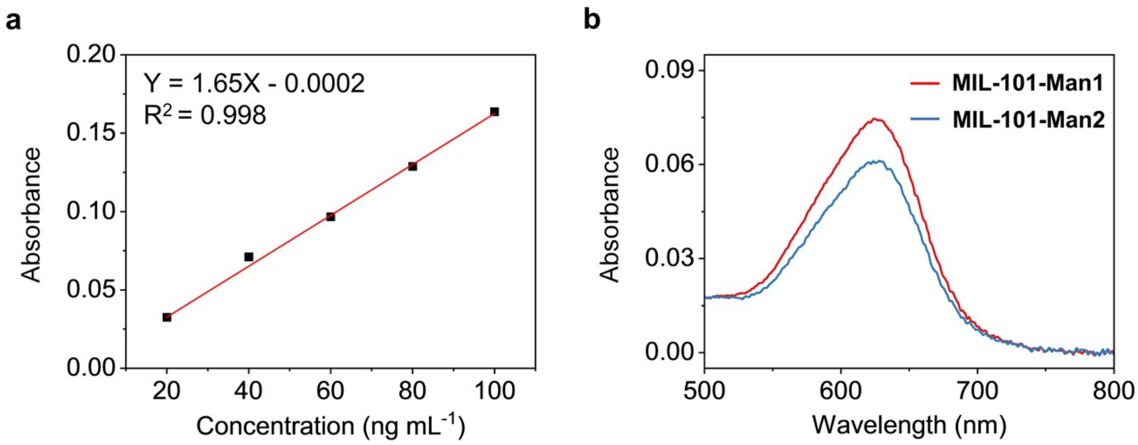

Figure S4. (a) Linear fitting curves for mannose treated with anthrone solution (0.5 wt% in 98% sulfuric acid), and the absorbance at 620 nm of the solution was measured. (b) UV-vis absorption spectra of **MIL-101-Man1** (0.1 mg mL^{-1}) and **MIL-101-Man2** (0.1 mg mL^{-1}).

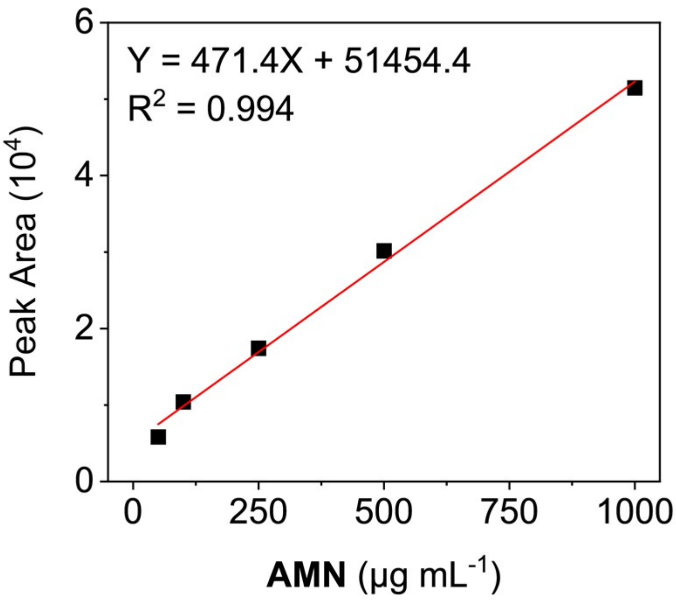

Figure S5. Calibration curve of **AMN** established by HPLC analysis. An **AMN** solution was prepared in H_2O/acetonitrile (1:1, v/v) and then filtered through 0.22 µm PTFE filters before injecting into HPLC equipped with PDA and D2 Lamps for reverse-phase HPLC. To calculate loading rates, we measured the non-encapsulated (leftover) **AMN** in the supernatant. Samples were run on a Phenomenex C18 column at 40 °C and detected at 210 nm. The mobile phase consisted of 100% water (A) and 100% acetonitrile (B) at an isomerization ratio of (A: B = 3:7) and a flow rate of 1 mL min^{-1}.

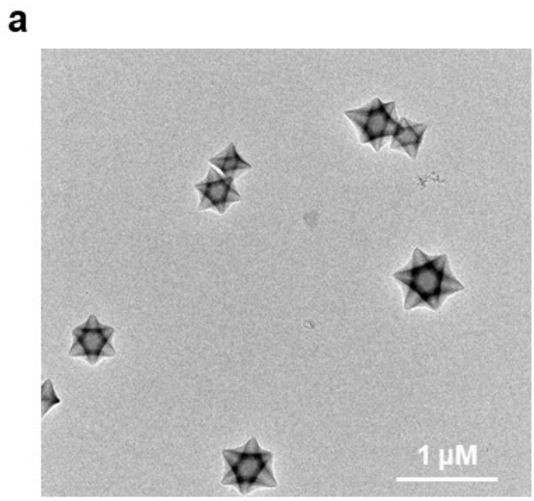

Figure S6. TEM image of (a) **AMN/MIL-101-Man1** (10 μg mL^{-1}) and (b) **AMN/MIL-101-Man2** (10 μg mL^{-1}).

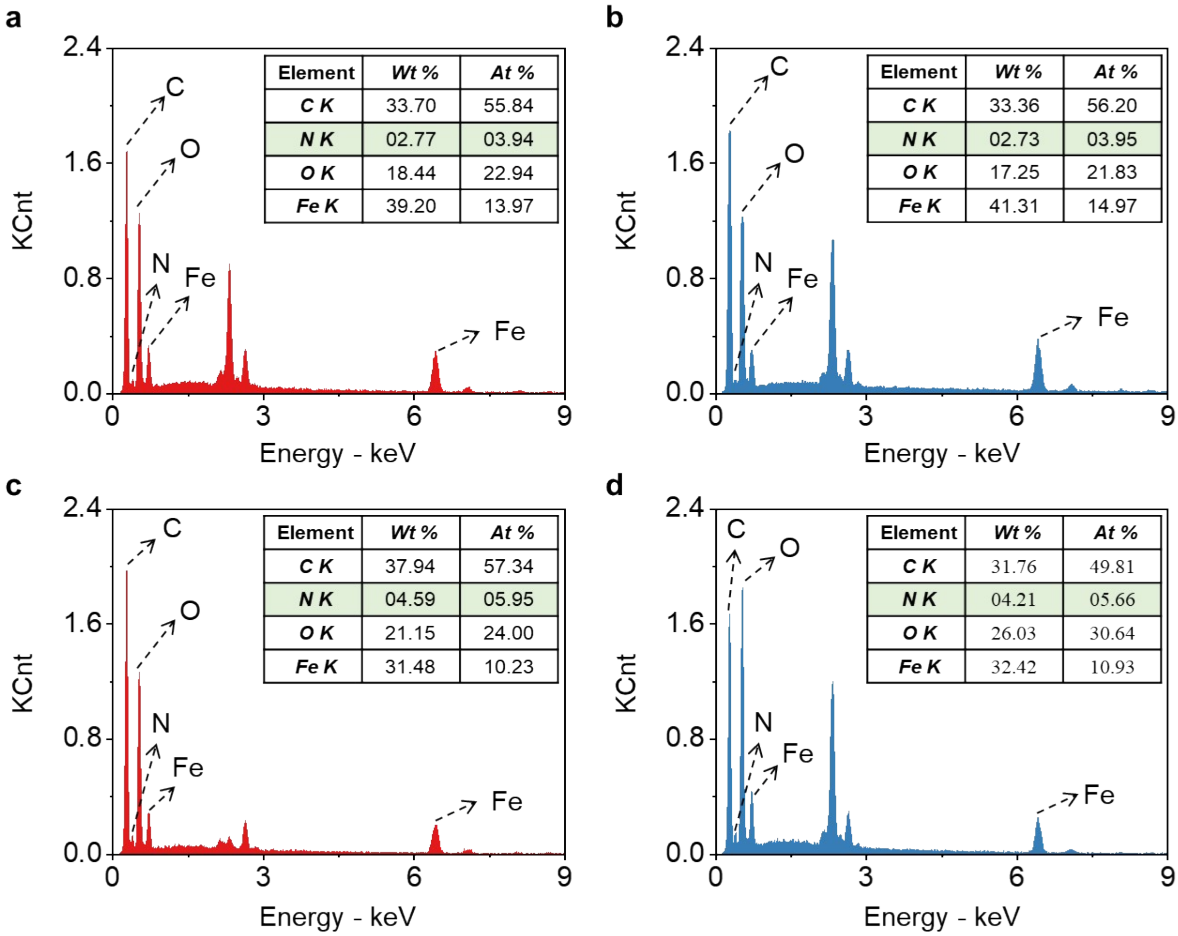

Figure S7. Quantitative elemental analysis of different MOFs including (a) **MIL-101-Man1**, (b) **MIL-101-Man2**, (c) **AMN/MIL-101-Man1** and (d) **AMN/MIL-101-Man2**.

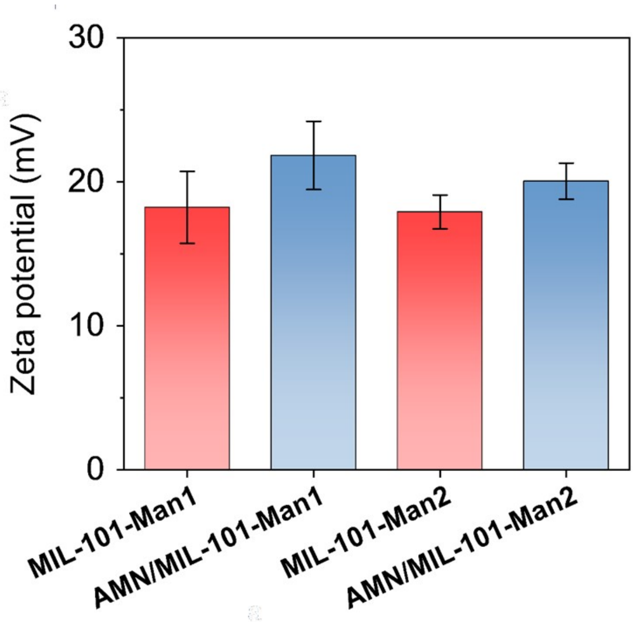

Figure S8. Zeta potential of **MIL-101-Man1** (0.1 mg mL^{-1}), **AMN/MIL-101-Man1** (50 μM/0.1 mg mL^{-1}), **MIL-101-Man2** (0.1 mg mL^{-1}) and **AMN/MIL-101-Man2** (55 μM/0.1 mg mL^{-1}).

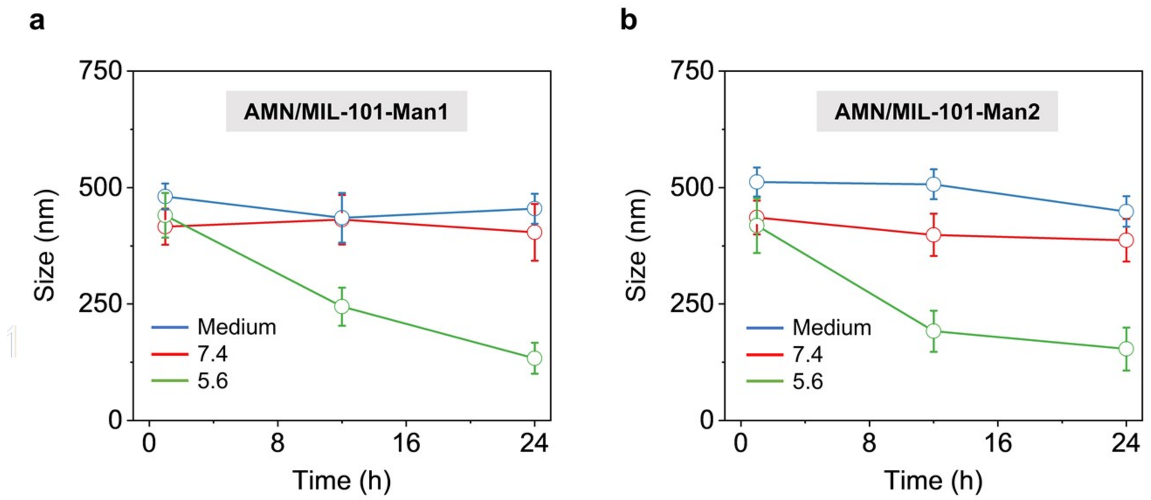

Figure S9. Changes in hydrodynamic diameter of **AMN/MIL-101-Man1** and **AMN/MIL-101-Man2** with time incubated in different solutions including pH 5.6 PBS solution, pH 7.4 PBS solution, and culture medium.

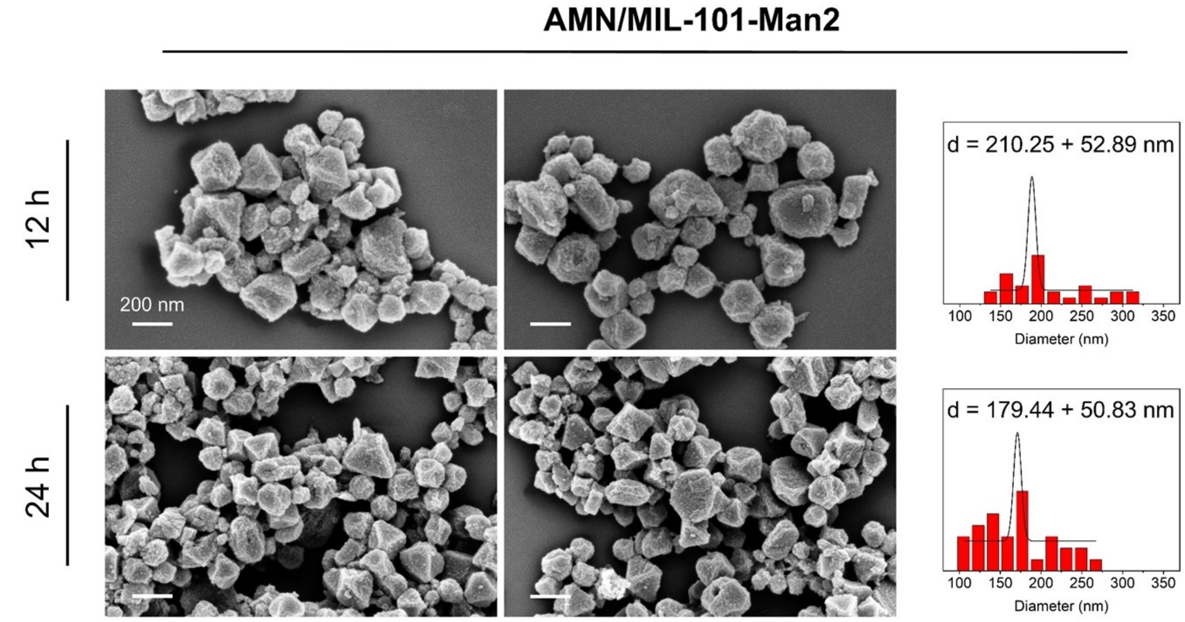

Figure S10. SEM image and particle size distribution of **AMN/ML2** (0.1 mg mL^{-1}) after 12 or 24 h incubation in PBS (0.01 M, pH 5.6).

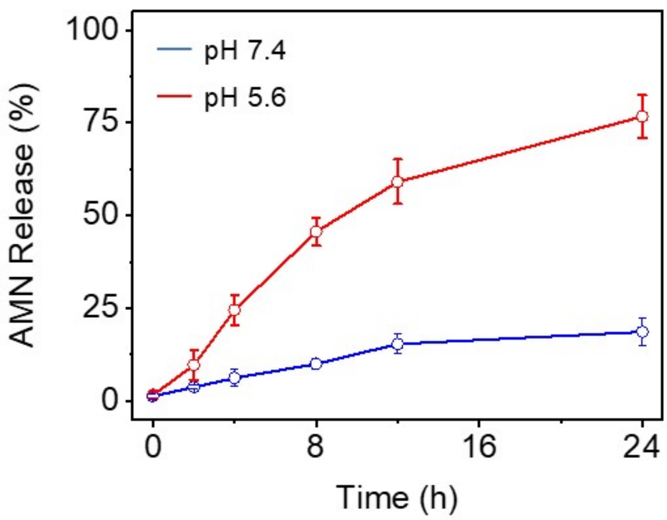

Figure S11. Measuring the released amount of **AMN** from **AMN/MIL-101-Man2** with time by HPLC.

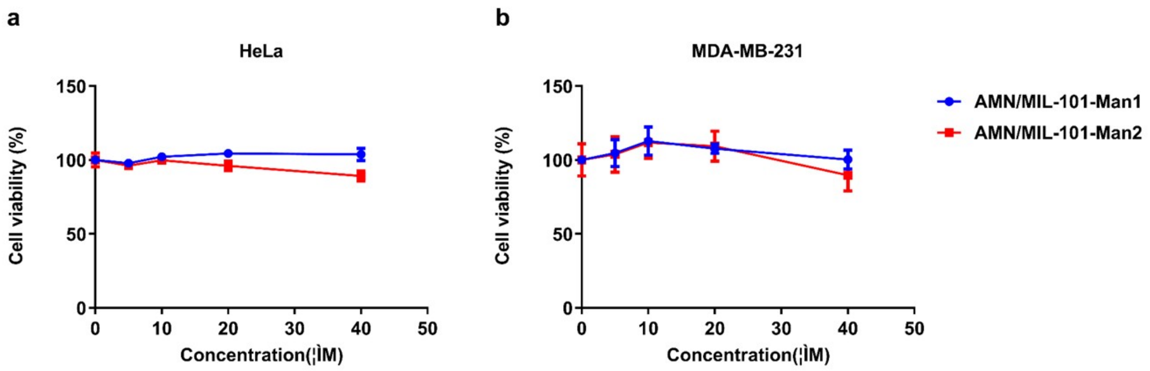

Figure S12. Viability of (a) HeLa and (b) MDA-MB-231 cells after 24 h incubation with **AMN/MIL-101-Man1** and **AMN/MIL-101-Man2** at different concentrations determined by the MTS cell proliferation assay. Error bars represent standard deviation (S. D., n = 3).

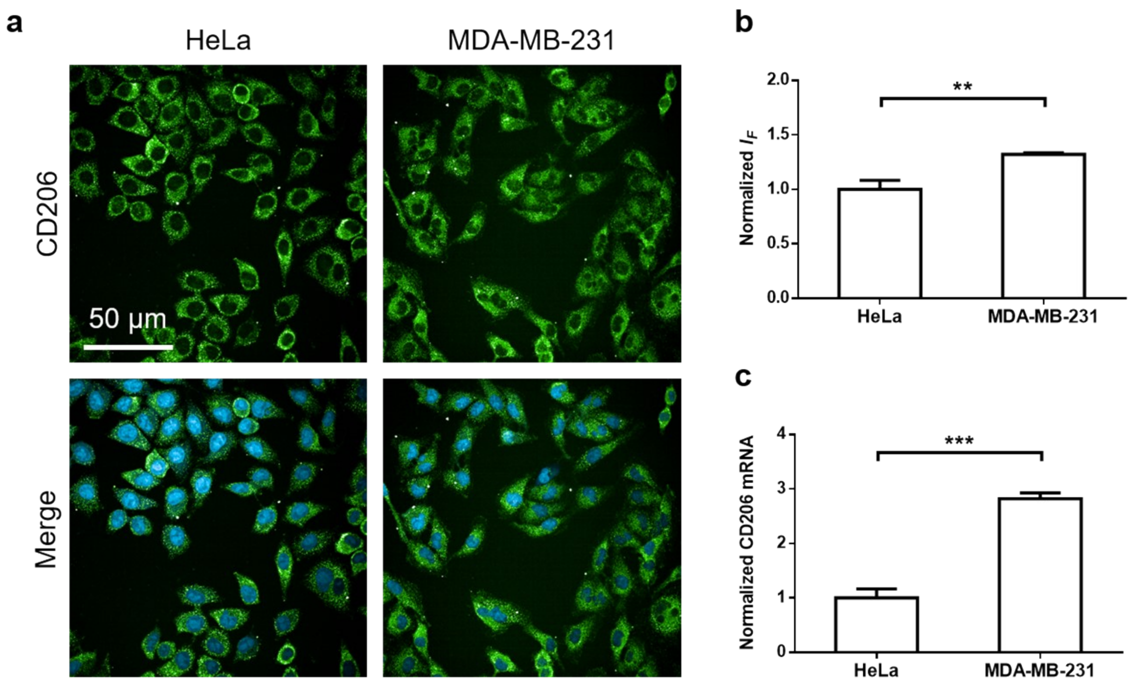

Figure S13. (a) Immunofluorescence staining and (b) quantification of HeLa and MDA-MB-231 cells using an anti-CD206 antibody. (c) Real-time qPCR measuring the CD206 mRNA in HeLa and MDA-MB-231 cells. Cell nuclei were stained with Hoechst 33342. Asterisks indicate significant differences (***P*<0.01 and ****P*<0.001).

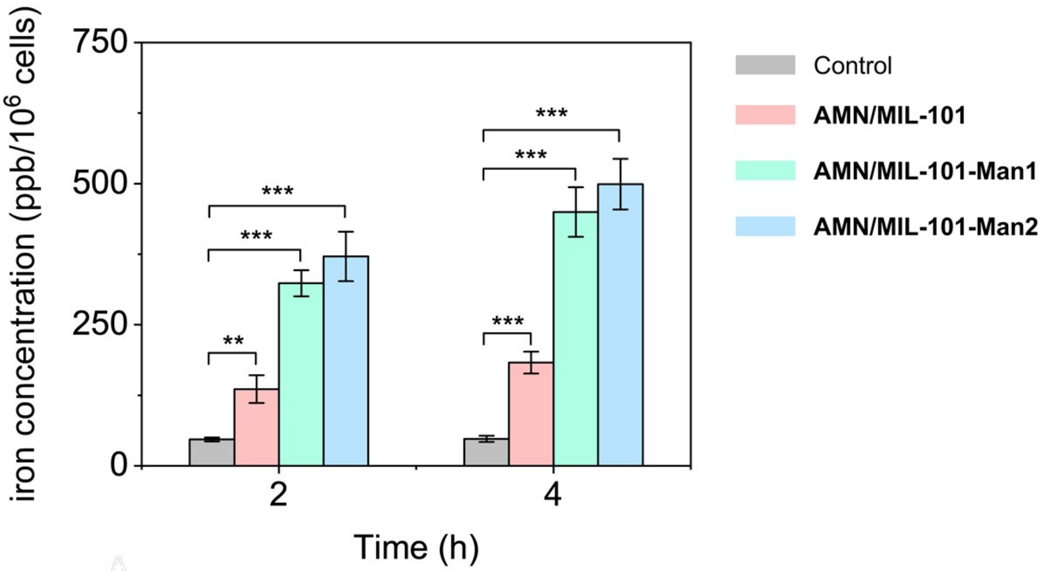

Figure S14. Quantitative analysis of intracellular iron concentrations in MDA-MB-231 cells after treatment with **AMN/MIL-101** (10 μg mL^{-1}), **AMN/MIL-101-Man1** (10 μg mL^{-1}) and **AMN/MIL-101-Man2** (10 μg mL^{-1}) at 2 h and 4 h. Asterisks indicate significant differences (**P<0.01, ***P<0.001).

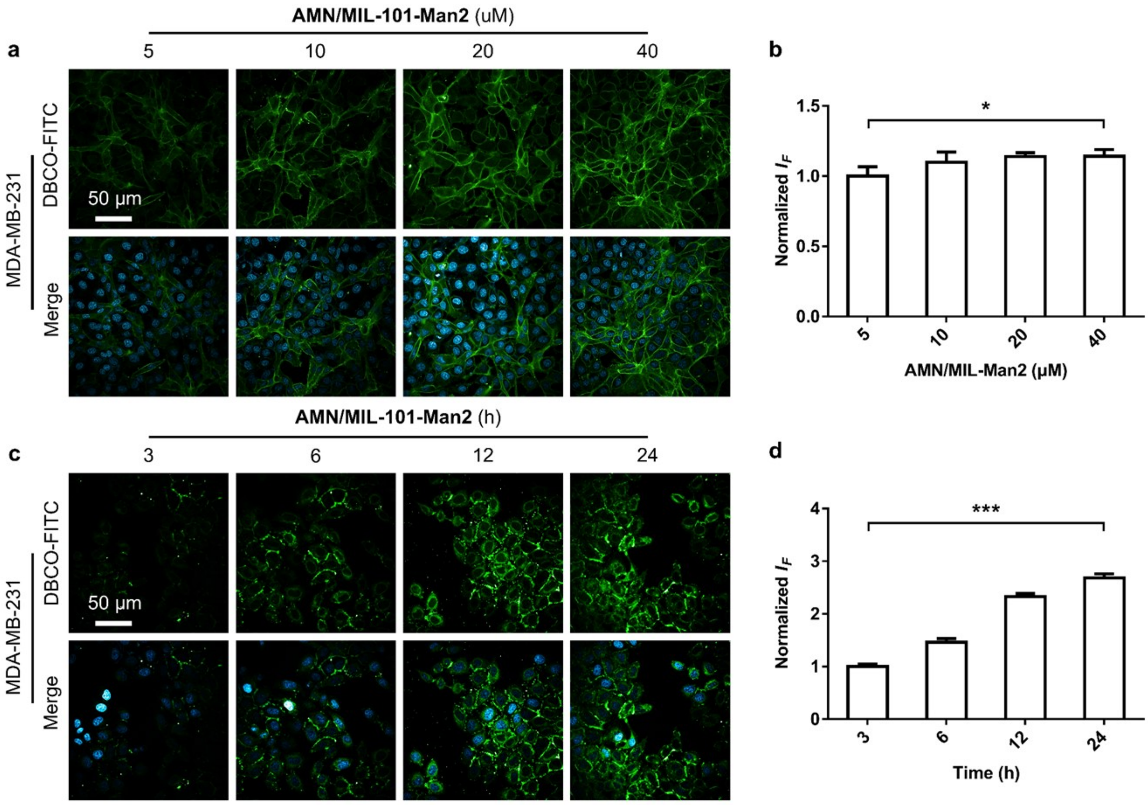

Figure S15. (a) Fluorescence imaging and (b) quantification of MDA-MB-231 cells treated with different concentrations of **AMN/MIL-101-Man2**. (c) Fluorescence imaging and (d) quantification of MDA-MB-231 cells treated with **AMN/MIL-101-Man2** (20 μM/36 μg mL^{-1}) with time. After treatment with the MOFs, the cells were fluorescently labeled with **DBCO-FITC** (10 μM) for 30 min. Cell nuclei were stained with Hoechst 33342. Asterisks indicate significant differences (**P*<0.05 and ****P*<0.001).

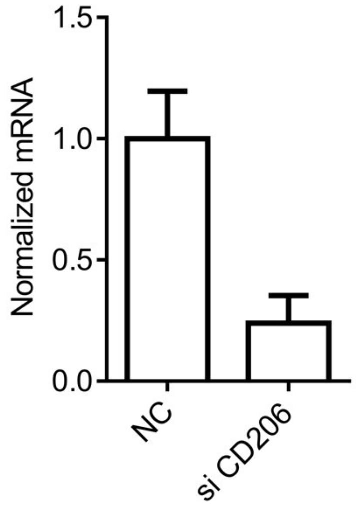

Figure S16. Quantitative real-time PCR applied to detect the CD206 mRNA expression level of MDA-MB-231 cells treated with si-CD206.

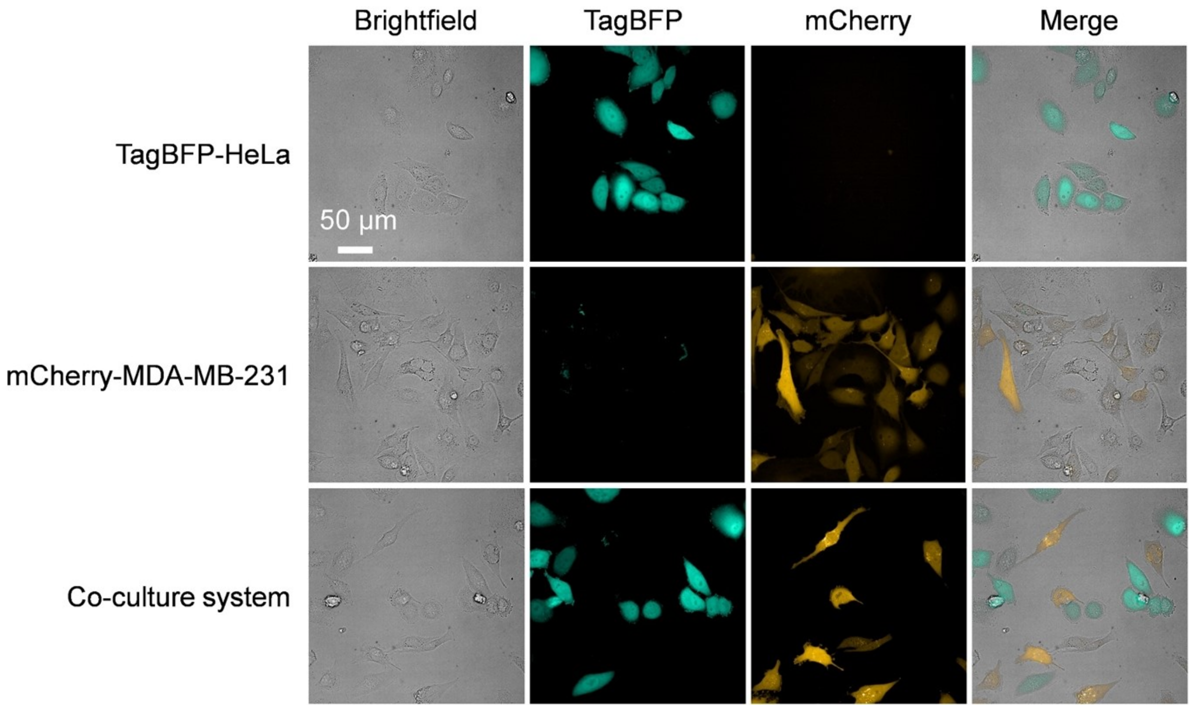

Figure S17. Fluorescence imaging of mCherry-MDA-MB-231 and TagBFP-HeLa cells applying different excitation/emission channels. When the excitation channel of TagBFP (405 nm) was applied, a fluorescence emission signal was detected in the corresponding TagBFP emission channel (435-480 nm), but not in the mCherry emission channel (580-620 nm); conversely, when the excitation channel of mCherry (561 nm) was applied, a fluorescence emission signal was detected in the corresponding mCherry emission channel (580-620 nm), but in the TagBFP emission channel (435-480 nm).

Table S1. Summary of the properties of reported delivery materials.

Delivery vector	**Delivery manner**	**Loading capacity**	**Controlled release**	**Ref**
Mannosyl MOFs	Active targeting	~20 wt%	pH responsive	**This work**
Lipidosome	Active targeting	~10 wt%	-	3-6
Hollow manganese dioxide	-	~60 wt%	GSH responsive	7
Chitosan nanoparticle	-	~20 wt%	-	8

Table S2. Summary of the loading efficiency of different MIL-101 carriers for small molecules.

MIL-101 carrier	**Payload**	**Loading efficiency (wt%)**	**Ref**
MIL-101-Man1	**AMN**	17.8 wt%	This work
MIL-101-Man2	**AMN**	19.1 wt%	This work
MIL-101-PLA-PEG-F3	Doxorubicin	16.8 wt%	9
LL-37@MIL-101	Vancomycin	25.0 wt%	10
MIL-101 (Fe)	Chlorantraniliprole	23.0 wt%	11
MIL-101(Fe)	Dihydroartemisinin	10.0 wt%	12
MIL-101-NH_2 (Fe)	Camptothecin	18.0 wt%	13
MIL-101-NH_2 (Fe)	Platinum-curcumin	18.5 wt%	14

S3. Spectra of new compounds

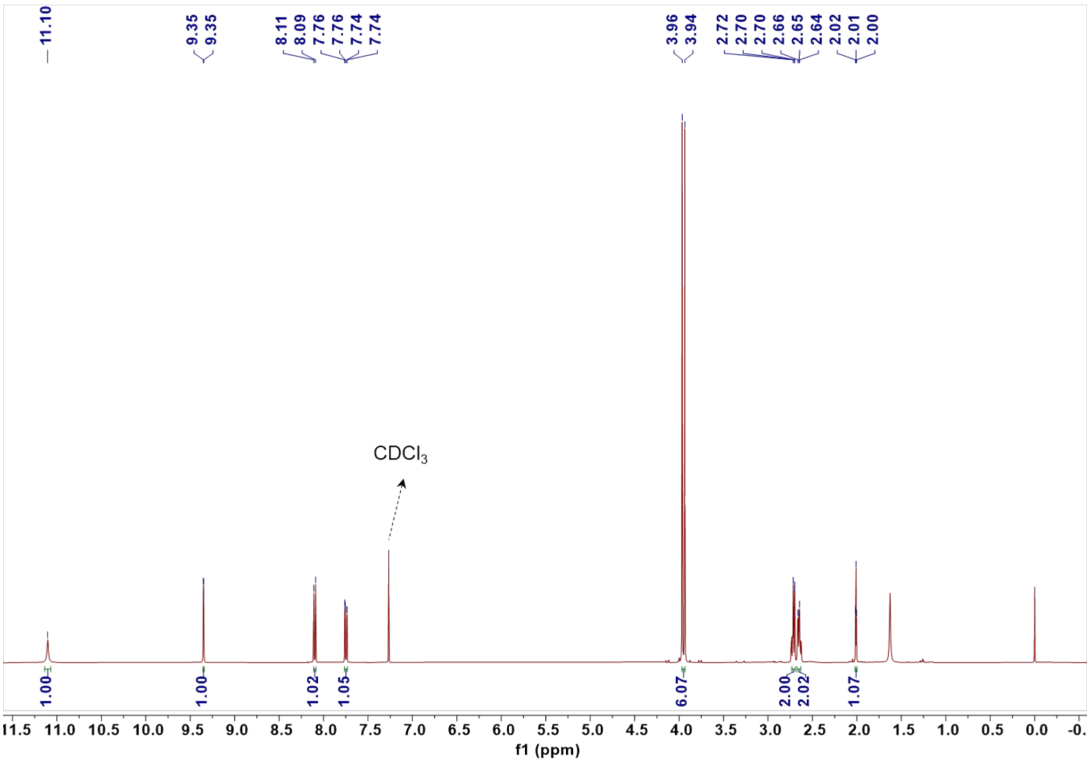

Figure S18. ^{1}H NMR spectrum of **3**.

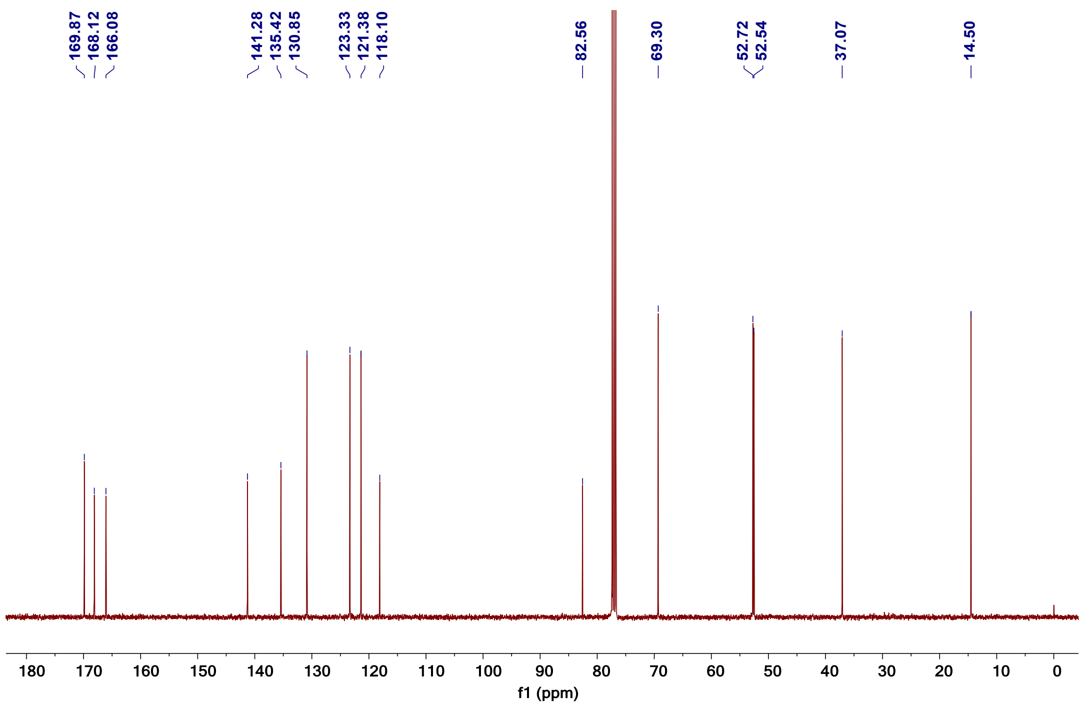

Figure S19. ^{13}C NMR spectrum of **3**.

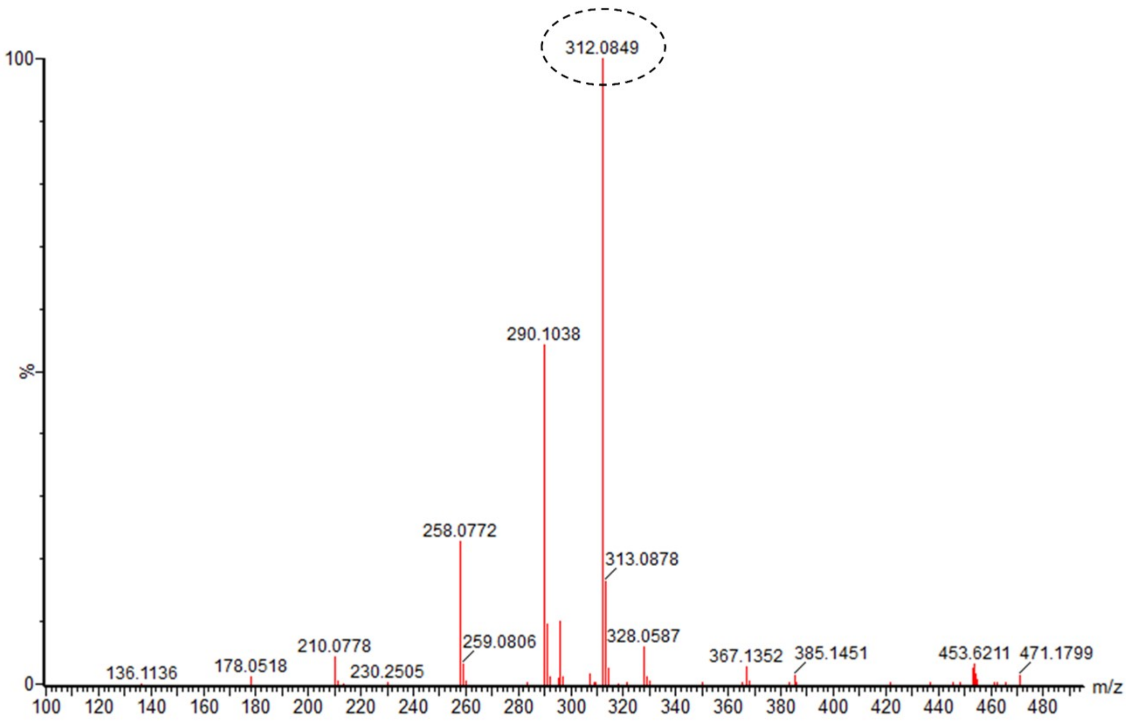

Figure S20. HRMS of **3**.

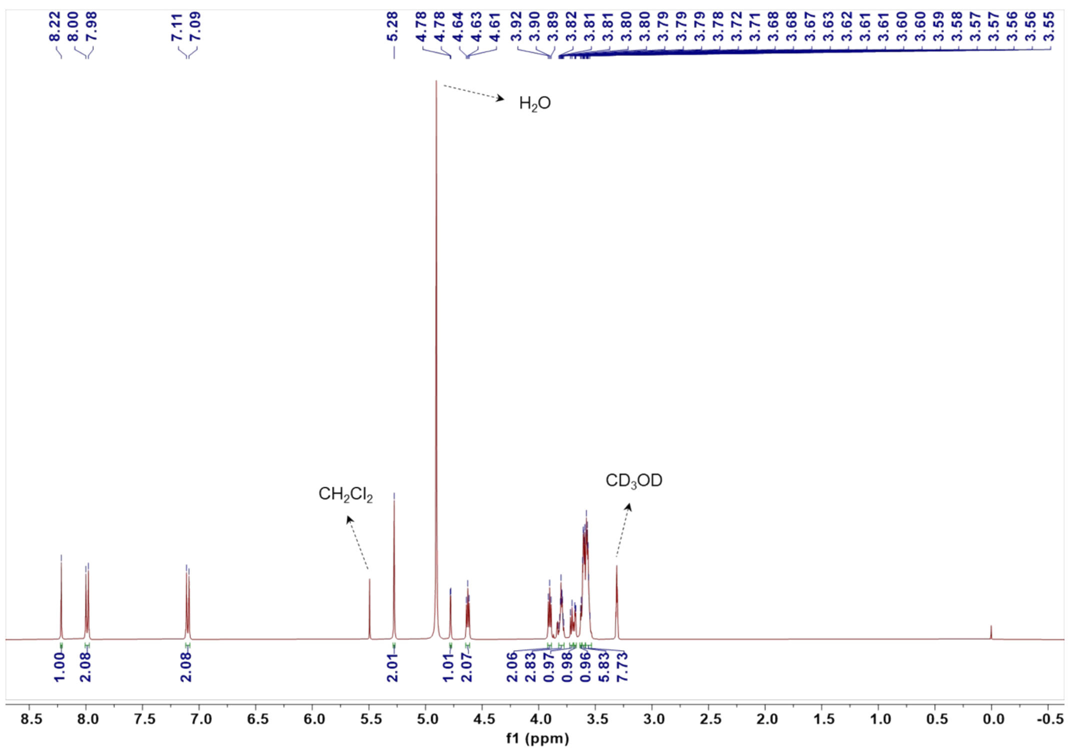

Figure S21. ^{1}H NMR spectrum of **Man-L1**.

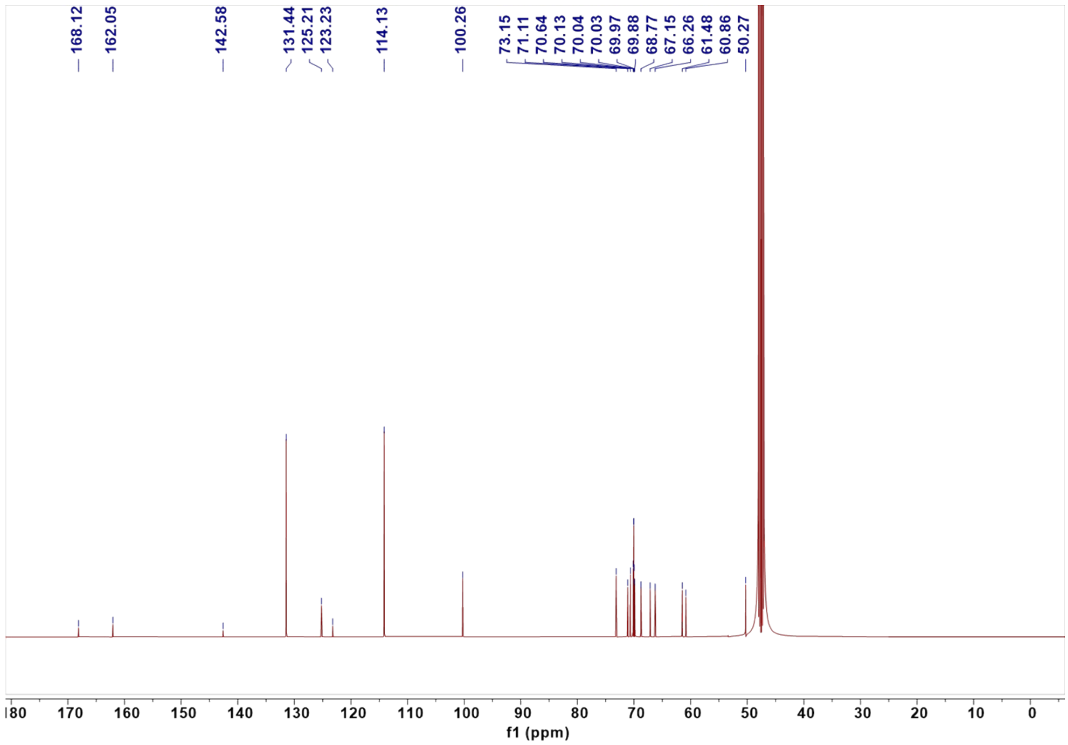

Figure S22. ^{13}C NMR spectrum of **Man-L1**.

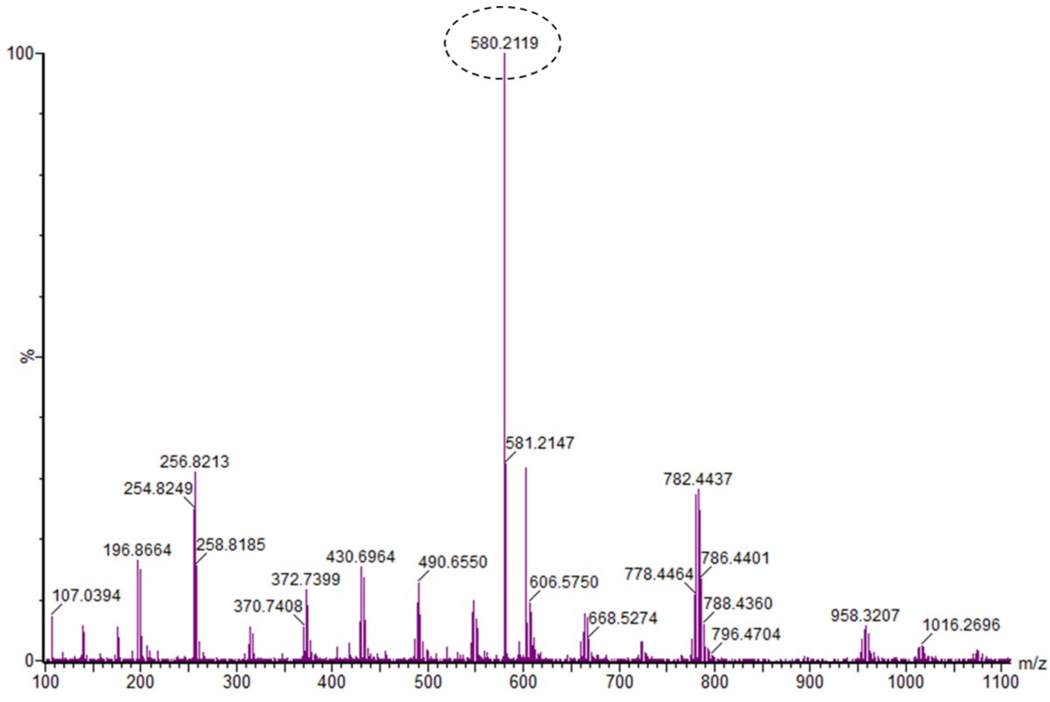

Figure S23. HRMS of **Man-L1**.

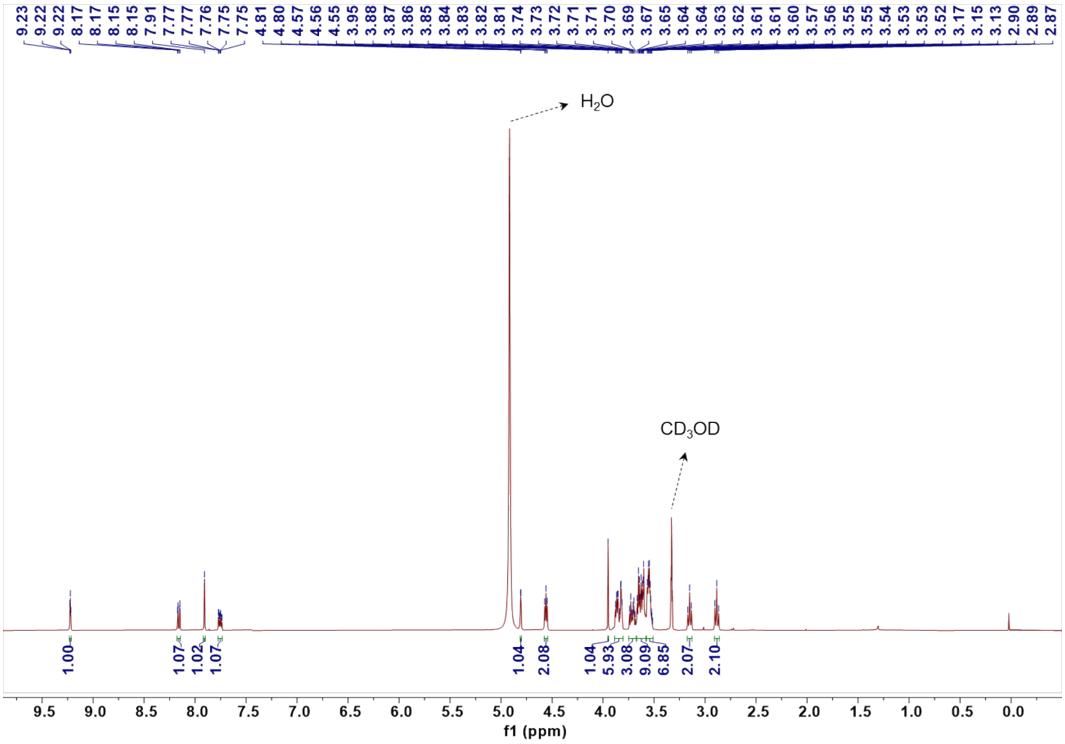

Figure S24. ^{1}H NMR spectrum of **Man-L2**.

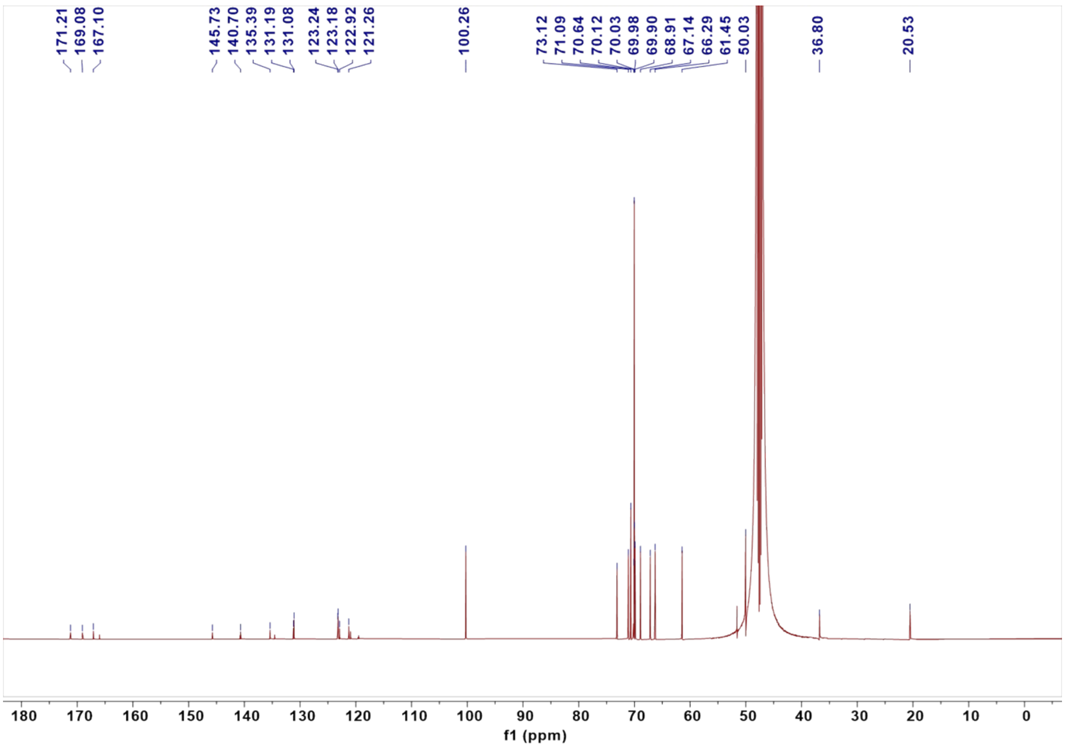

Figure S25. ^{13}C NMR spectrum of **Man-L2**.

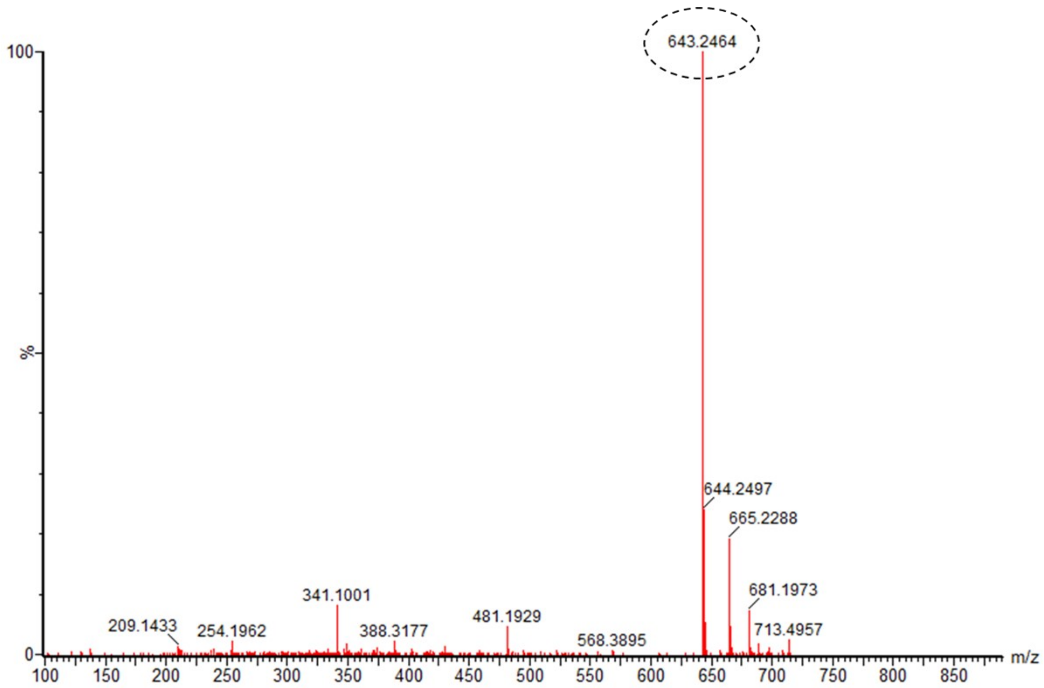

Figure S26. HRMS of **Man-L2**.

S4. Additional references

1. S. Zhang, R. Moussodia, H. Sun, P. Leowanawat, A. Muncan, C. D. Nusbaum, K. M. Chelling, P. A. Heiney, M. L. Klein, S. Andre, R. Roy, H. Gabius and V. Percec, *Angew. Chem. Int. Ed*., 2014, **126**, 11079-11083.
2. J. Zhang, Y. Li, F. Zhang, C. Hu and Y. Chen, *Angew. Chem. Int. Ed*., 2015, **55**, 1872-1875.
3. Z. Liu, F. Wang, X. Liu, Y. Sang, L. Zhang, J. Ren and X. Qu, *Proc. Natl. Acad. Sci. U. S. A.*, 2021, **118**, e2022769118.
4. R. Xie, S. Hong, L. Feng, J. Rong and X. Chen, *J. Am. Chem. Soc.*, 2012, **134**, 9914-9917.
5. R. Xie, L. Dong, R. Huang, S. Hong, R. Lei and X. Chen, *Angew. Chem. Int. Ed.*, 2014, **53**, 14082-14086.
6. Y. Sun, S. Hong, R. Xie, R. Huang, R. Lei, B. Cheng, D.-e. Sun, Y. Du, C. M. Nycholat and J. C. Paulson, *J. Am. Chem. Soc.*, 2018, **140**, 3592-3602.
7. J. Yang, K. Yang, S. Du, W. Luo, C. Wang, H. Liu, K. Liu, Z. Zhang, Y. Gao and X. Han, *Angew. Chem. Int. Ed.*, 2023, **62**, e202306863.
8. S. Lee, H. Koo, J. H. Na, S. J. Han, H. S. Min, S. J. Lee, S. H. Kim, S. H. Yun, S. Y. Jeong and I. C. Kwon, *ACS Nano*, 2014, **8**, 2048-2063.
9. J. Liu, Y. Cong, Y. Zeng, Y. He, Y. Luo, W. Lu, H. Xu, Y. Yin, H. Hong and W. Xu, *J. Appl. Polym. Sci.,* 2022, **140**, e53408.
10. L. Luogen, Z. Wanqing, Z. Yan, T. Yuanbiao, L. Simeng, X. Tongxuan, Z. Tianyue, X. Shan, Z. Pengwu, P. Qingshan and Z. Wufu, *Chem. Eng. J.,* 2022, **435,** 135084.
11. Y. Gao, Y. Liang, Z. Zhou, J. Yang, Y. Tian, J. Niu, G. Tang, J. Tang, X. Chen, Y. Li and Y. Cao, *Chem. Eng. J.,* 2021, **422**, 130143.
12. C. Wang, X. Jia, W. Zhen, M. Zhang and X. Jiang, *ACS Biomater. Sci. Eng.,* 2019, **5**, 4435-4441.
13. A. Cabrera-García, E. Checa-Chavarria, E. Rivero-Buceta, V. Moreno, E. Fernández and P. Botella, *J. Colloid Interface Sci.,* 2019, **541**, 163-174.
14. M. M. Moradi, M. Aliomrani, S. Tangestaninejad, J. Varshosaz, H. Kazemian, F. Emami and M. Rostami, *Appl. Organomet. Chem.,* 2022, **36**, e6755.